# Suppression of Three-Dimensional Charge Density Wave Ordering via Thickness Control

Gideok Kim,[1,2] Michael Neumann,[1,2] Minu Kim,[1,2,*] Manh Duc Le,[1,2] Tae Dong Kang,[1,2] and Tae Won Noh[1,2,†]
[1]*Center for Correlated Electron Systems, Institute for Basic Science (IBS), Seoul 151-742, Republic of Korea*
[2]*Department of Physics and Astronomy, Seoul National University, Seoul 151-742, Republic of Korea*
(Received 16 July 2015; published 24 November 2015)

Barium bismuth oxide ($BaBiO_3$) is the end member of two families of high-$T_c$ superconductors, i.e., $BaPb_{1-x}Bi_xO_3$ and $Ba_{1-x}K_xBiO_3$. The undoped parent compound is an insulator, exhibiting a charge density wave that is strongly linked to a static breathing distortion in the oxygen sublattice of the perovskite structure. We report a comprehensive spectroscopic and x-ray diffraction study of $BaBiO_3$ thin films, showing that the minimum film thickness required to stabilize the breathing distortion and charge density wave is ≈11 unit cells, and that both phenomena are suppressed in thinner films. Our results constitute the first experimental observation of charge density wave suppression in bismuthate compounds without intentionally introducing dopants.

DOI: 10.1103/PhysRevLett.115.226402 PACS numbers: 71.45.Lr, 73.21.-b, 78.20.-e, 78.30.-j

The discovery of the oxide high-temperature superconductors $BaPb_{1-x}Bi_xO_3$ (BPBO), with a maximum $T_c = 13$ K [1], and $Ba_{1-x}K_xBiO_3$ (BKBO), with $T_c = 30$ K [2,3], led to much experimental and theoretical research interest in these materials [4–6]. BPBO, BKBO, and their semiconducting parent material $BaBiO_3$ (BBO) have a perovskite crystal structure, as shown in Fig. 1(a). As with layered cuprate high-$T_c$ superconductors, BPBO and BKBO become superconducting via $p$-type doping of a nonmetallic parent compound which exhibits long-range order. However, in contrast to the antiferromagnetically ordered Mott insulators formed by the cuprate parent compounds, undoped BBO is a charge-disproportionated charge-density-wave (CDW) insulator with no magnetic moments [4–6].

The presence of two nonequivalent Bi sites is reflected in the effective sum formula $Ba_2Bi^{4+\delta}Bi^{4-\delta}O_6$, with $Bi^{4+\delta}$ and $Bi^{4-\delta}$ ions occupying alternating $BiO_6$ octahedra of different sizes, as shown in Fig. 1(b). This ionic arrangement can be viewed as long-range CDW ordering [7]. The so-called breathing lattice distortion associated with the presence of two distinct Bi-O bond lengths is stabilized by an oxygen breathing phonon mode with the same symmetry, which involves the symmetric motion of oxygen atoms residing on the vertices of the $BiO_6$ octahedra, as shown in Fig. 1(a) [8,9]. The same breathing mode also mediates Cooper pairing in the superconducting phases of BPBO and BKBO [8,10,11].

The complex interplay of lattice distortions and the electronic behavior of bismuthates remains an active area of research [12–20]. However, few control parameters are available to manipulate these lattice distortions experimentally. The phase diagram of bulk BBO is commonly explored via chemical doping of K atoms into Ba sites, or Pb atoms into Bi sites [4,21,22]. However, such substitutional doping leads to several effects: besides introducing a single $p$-type carrier per substituted atom, it also leads to chemical pressure because the ionic radii of K and Pb are smaller than those of Ba and Bi, respectively. Furthermore, doping introduces a degree of disorder to the parent material. It is therefore challenging to separate these effects, and to determine which governs the complex interaction between lattice distortions and the electronic properties of BBO. For these reasons, it is desirable to identify other experimental methods to control the breathing lattice distortion and study the influence on the electronic structure of BBO.

Here we explore the possibility to modify the properties of BBO by tuning a different control parameter: we vary the dimensionality of the sample by controlling the thickness of stoichiometric BBO films. The rationale behind this approach is the expectation that the three-dimensional (3D) CDW pattern is stable only above a certain length scale $d_c$, and that if we impose a sample thickness $d < d_c$, we may expect to stabilize a distinct phase of BBO. This approach has the advantage that it avoids doping-induced disorder, and that the nominal density of charge carriers remains unchanged.

We grew high-quality BBO films on (001) $SrTiO_3$ (STO) substrates using pulsed laser deposition, and varied the film thickness from 2 to 170 unit cells (u.c.). Throughout this Letter, we refer to these film samples as $n$-BBO, where $n$ is the number of BBO unit cells. Sample characterization was carried out using *in situ* reflection high-energy electron diffraction (RHEED), atomic force microscopy (AFM), and Rutherford backscattering, and reveals that our epitaxial growth resulted in BBO films with a very smooth surface and good stoichiometry (see the Supplemental Material for further details [23]).

We investigated the structure of the BBO films using high-resolution x-ray diffraction (XRD). The resulting $\theta - 2\theta$ patterns are shown in Fig. 1(c), and comprise only (00l) reflections from STO and BBO, demonstrating that

 

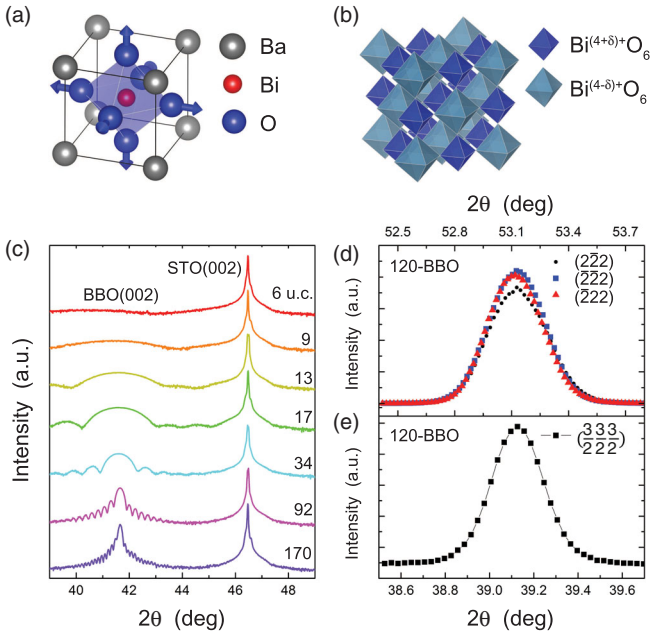


FIG. 1 (color online). Structural characterization of the BBO films. (a) A schematic diagram of the perovskite lattice structure. The blue arrows show the atomic motion associated with the oxygen breathing phonon mode. (b) A schematic diagram of the static breathing distortion, showing the three-dimensional checkerboard ordering of nonequivalent $BiO_6$ octahedra. (c) XRD $\theta$-$2\theta$ patterns, showing the (002) reflections of BBO and the STO substrates for film thicknesses in the range 6–170 u.c. The measurements employed the Cu $K_\alpha$ line. (d) XRD $\theta$-$2\theta$ patterns of thick 120-BBO, showing the (222) series of reflections. (e) The presence of a static breathing distortion results in a doubling of the unit cell, as well as the appearance of a half-integer $(3/2, 3/2, 3/2)$ reflection. The data in (d),(e) were acquired using a synchrotron source with $E = 11.03$ keV. All reflections are indexed to pseudocubic notation.

the films were oriented along the $c$ axis. The presence of numerous interference fringes around the BBO (002) reflection confirms that the surface of the films and the substrate interface were flat, which is consistent with RHEED and AFM analysis [23]. We use the modulation period to determine the film thicknesses. Films that were $\geq$ 13-u.c. thick exhibited a pseudocubic lattice parameter of $c = 4.334 \pm 0.008$ Å, which is close to that previously reported for bulk BBO [21] and BBO films [26–28]. Figure 2(a) shows an XRD reciprocal space map (RSM) of 120-BBO that covers the vicinity of the STO (103) reflection. This measurement established that thick BBO films had an in-plane lattice parameter of $a = 4.377$ Å, which is comparable to that of bulk BBO. Significantly, the RSM reveals that the reflections due to BBO and the STO substrate were well separated, demonstrating that the BBO film was fully relaxed, i.e., was not strained due to lattice mismatch with the substrate.

We further analyzed the lattice structure of the thick 120-BBO film using XRD patterns obtained using a synchrotron radiation source. To identify tilting distortions of the perovskite lattice, we performed $\theta - 2\theta$ scans of the (222) series of reflections, as shown in Fig. 1(d). All diffraction maxima occurred at the same angle, indicating that 120-BBO exhibits a tetragonal lattice structure. This result differs from the behavior of bulk BBO, which has a monoclinic lattice structure [21,23]. The presence of static breathing distortion leads to the appearance of half-integer reflections in diffraction experiments, due to an effective doubling of the unit cell. Figure 1(e) shows a prominent maximum in a $\theta$–$2\theta$ scan at the reciprocal lattice index $(3/2, 3/2, 3/2)$. This observation provides unambiguous evidence that a static breathing distortion was present in 120-BBO, which is consistent with the results of a previous study [28].

To probe for possible structural changes in the BBO films as a function of thickness, we performed XRD RSM scans centered on the BBO (103) reflection. We find that for films with a thickness of 120, 17, and 13 u.c., the out-of-plane and in-plane lattice parameters underwent only minor changes, as shown in Figs. 2(b)–2(d), accompanied by a broadening of the reflection, which is attributed to the finite sample thickness. In particular, the reflection maxima deviated from the dashed line that describes the reciprocal lattice points at which the in-plane and out-of-plane lattice constants are equal, demonstrating that the lattice distortions were retained throughout this thickness range. By contrast, as shown in Fig. 2(e), a shift in this reflection occurred for the 9-BBO film, indicating an abrupt 1% increase in the $c$-axis parameter. The observed lattice spacings of $a = c = 4.377$ Å suggest that a structural transition to a cubic structure occurred as the film thickness decreased from 13 to 9 u.c.

Raman spectroscopy provides a sensitive means of observing lattice distortions in BBO. The symmetric oxygen breathing phonon mode that provides the coupling between the lattice and electronic properties of BBO has $A_g$ symmetry, and this mode is Raman active if tilting is present, or if static breathing distortions of the perovskite lattice are present. In contrast, in the absence of such lattice distortions, no phonon modes are Raman active. Previous work by Tajima *et al.* [29] showed that the first-order breathing mode at $\approx$565 $cm^{-1}$ dominates the Raman spectra of undoped BBO, and that the intensity of this mode is at a maximum for incident radiation with $\lambda = 633$ nm ($\simeq$1.96 eV), i.e., in resonance with the optical band gap. As the doping density of potassium increases, the amplitude of the Raman response at 565 $cm^{-1}$ gradually reduces, and it vanishes at $x \simeq 0.4$, where a transition to a cubic $Pm\bar{3}m$ lattice structure occurs [23].

Figure 3(a) shows Raman spectra of the undoped BBO films studied in this work, which exhibited a marked evolution as the film thickness decreased. The Raman spectrum of the thick 130-BBO film is dominated by the

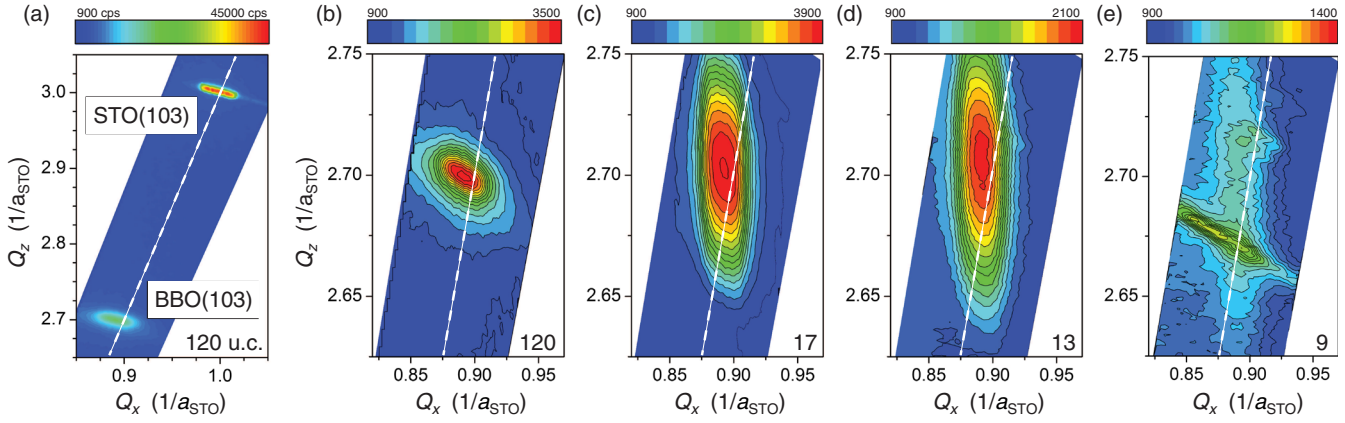


FIG. 2 (color online). XRD reciprocal space maps of the BBO films, acquired using (103) reflections. The reciprocal coordinates are provided in terms of the substrate lattice parameter $a_{STO} = 3.905$ Å. The dashed lines indicate the positions of (103) reflections expected for an undistorted cubic lattice. (a) A thick 120-BBO film. The reflections from the substrate and from BBO are well separated, demonstrating that the BBO film is relaxed. (b)–(e) Evolution of the BBO (103) reflections with the film thickness. (b) 120, (c) 17, (d) 13, and (e) 9 u.c. The color scale was adjusted separately for each sample.

first-order breathing mode at 565 $cm^{-1}$. As the film thickness $d$ was reduced, the relative intensity of the signal from the STO substrate increased, whereas the Raman intensity of the breathing mode gradually diminished. However, at $d = 9$ u.c., the Raman response of BBO films was suppressed completely. A magnified view [see Fig. S3(b) in the Supplemental Material [23]] reveals that the Raman spectra of films that were ≤9-u.c. thick were indistinguishable from the spectrum of the STO substrate. This complete suppression of the Raman response below a threshold thickness of $d_c = (11 \pm 2)$ u.c. is highlighted in Fig. 3(b), and provides further evidence for a structural transition to a cubic $Pm\bar{3}m$ phase in which no phonons are Raman active.

The formation of long-range CDW in bulk BBO leads to a band gap at the Fermi level [12,15,16,20]. Several authors have reported a prominent maximum in the optical conductivity $\sigma_1(\omega)$ at around 2 eV, and have attributed this spectral feature to the presence of CDW ordering [30–32]. To track the evolution of charge ordering as a function of the sample thickness $d$, we measured $\sigma(\omega)$ for our BBO films via spectroscopic ellipsometry. As shown in Fig. 3(d), we observed a strong peak at ≃2 eV in the spectrum of the thick 92-BBO film. As we decreased $d$ to 34, 17, and

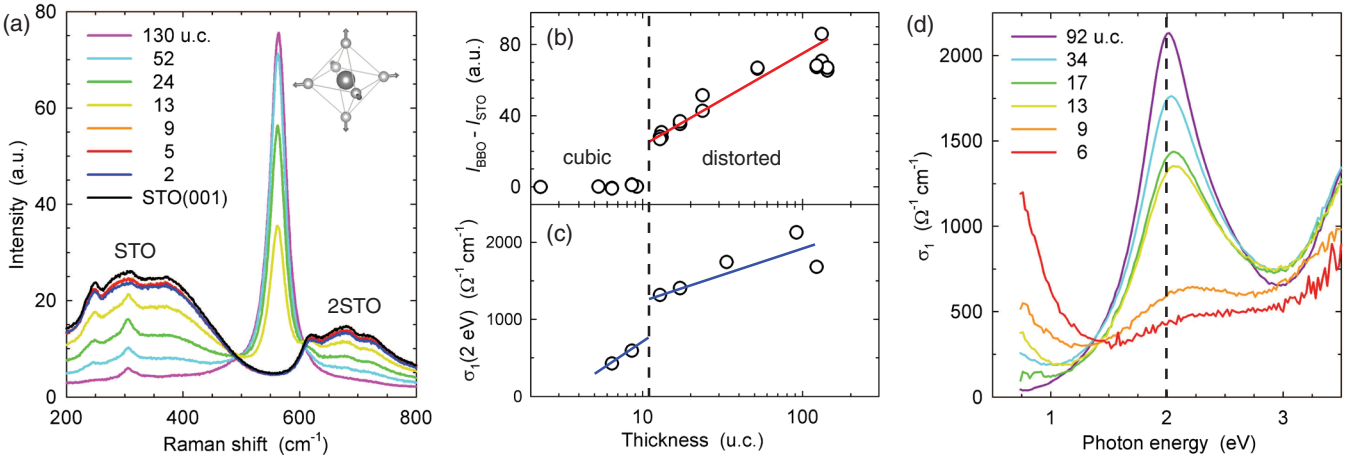


FIG. 3 (color online). Spectroscopic characterization of the BBO films. (a) The Raman response at $\lambda = 633$ nm. The spectral features comprise a mode at ~565 $cm^{-1}$, which results from the BBO oxygen breathing phonon (see the inset), as well as first- and second-order modes of the substrate (STO, 2STO). For $d \leq 9$ u.c., the oxygen breathing mode is not Raman active. (All Raman spectral data are shown as measured without normalization or vertical shifts.) (b) The amplitude of the Raman response for the oxygen breathing mode relative to the STO response baseline. (c) The evolution of optical conductivity at the absorption maximum, $\sigma_1(2\text{ eV})$, with sample thicknesses. The dashed line highlights discontinuous behavior at $d_c \simeq 11$ u.c. The solid lines are guides to the eye. (d) The optical conductivity $\sigma_1$ measured via spectroscopic ellipsometry. The absorption maximum at ~2 eV marked by the dashed line reflects the CDW gap in BBO.

13 u.c., the amplitude of this peak in $\sigma_1(\omega)$ gradually decreased. Further thickness reduction led to a strong suppression of this peak, leaving only an indistinct and broad feature in $\sigma(\omega)$ for 9-BBO and 6-BBO, which is indicative of a melting of CDW order. The thickness dependence of $\sigma_1(\omega)$ at 2 eV shown in Fig. 3(c) suggests that this melting of charge order occurs as a sudden transition at a critical thickness in the range 9–13 u.c., which coincides with the structural transition to a cubic $Pm\bar{3}m$ lattice evidenced by the disappearance of the Raman activity of the oxygen breathing phonon mode, as shown in Fig. 3(b).

Varying the thickness provides a means to control CDW ordering in BBO without the complexities associated with extrinsic doping. In bulk BKBO, increasing the doping density $x$ leads to a progressive reduction in the optical band gap energy to below 2 eV [30,32] and to the appearance of an additional peak at around 0.85 eV due to the formation of bipolarons [13,32] (see, for example, Fig. 1 in Ref. [32]). Neither effect is visible in the spectra acquired for the BBO films, for which the absorption maximum remained at 2 eV regardless of the film thickness. This important difference highlights the distinct advantage of thickness control, which avoids the introduction of additional charge carriers or disorder into BBO films.

Taken together, our XRD, ellipsometry, and Raman spectroscopy observations provide considerable insight into the effects of thickness on the BBO films. For $d > d_c \simeq$ 11 u.c., the films exhibit a structural distortion due to tilting of the $BiO_6$ octahedra, as well as a static breathing distortion that comprises two nonequivalent Bi sites and a concomitant CDW, analogous to the case of bulk BBO. With $d < d_c$, however, the tilting and breathing distortions abruptly disappear, accompanied by suppression of the CDW. We conclude that $d_c = (11 \pm 2)$ u.c. represents a critical length scale for the stability of the 3D checkerboard CDW pattern in BBO [see Fig. 1(b)]. Intriguingly, the length scale observed in our study is comparable to the typical grain size of the tetragonal polymorph found in BPBO single crystals, as well as to the superconducting coherence length at optimal doping [33], which suggests that real-space and momentum-space pairing in the bismuthates share a common characteristic length scale.

Previous experimental and theoretical work has consistently shown that, in the absence of lattice distortions, the cubic $Pm\bar{3}m$ phases of bismuthates are metallic [4–6]. This suggests that the sudden disappearance of lattice distortions in BBO thin films at $d_c = 11$ u.c. may be accompanied by an insulator-to-metal transition. This accords with the observation that in the optical conductivity spectra shown in Fig. 3(d), concurrently with the suppression of the peak at 2 eV, a Drude-like peak appears at energies below ~1 eV; this transfer of spectral weight in $\sigma_1(\omega)$ may signal an incipient thickness-controlled insulator-to-metal transition, analogous to the behavior observed in bulk BPBO and BKBO. In electrical transport measurements, thick BBO films are insulating, as expected. However, so far no reliable measurements have been obtained for $d < d_c$. This may be due to contact-induced oxygen depletion; however, an alternative, speculative scenario is suggested by the observation that at $d < d_c$, the peak in $\sigma_1(\omega)$ at 2 eV is not completely suppressed. While the oxygen breathing phonon mode is Raman inactive in the undistorted $Pm\bar{3}m$ lattice, it might still provide sufficient coupling to stabilize residual CDW order in this thickness regime, which may compete with the incipient metallic state. Further measurements are in progress to clarify this phenomenon.

In this Letter, we have demonstrated that the CDW ordering of BBO can be suppressed by varying the thickness of the BBO film. This phenomenon differs conceptually from dimensional control using quantum confinement effects [34–36]: rather than directly limiting the space available to free carriers, varying the film thickness $d$ alters the relative stability of different BBO lattice structures and CDW ordering patterns, with a crossover occurring at $d = d_c$. This scenario can likely be tested by extending existing DFT calculations for bulk BBO [12–20] to BBO slabs of several unit cells thickness. The extent to which the STO substrate is involved in the suppression of CDW order observed at $d < d_c$ is unclear so far. In the case of fully strained FeSe films deposited epitaxially on STO substrates, coupling of optical phonons of STO to the electrons of FeSe has been reported to enhance the superconducting transition temperature of FeSe monolayers to 109 K [37,38]. However, in contrast to the case of FeSe, BBO films grown on STO are fully relaxed, suggesting a weaker influence of the substrate.

Film thickness control over the phase stability, such as demonstrated in this work, is expected to be valuable in the search for emergent phenomena in transition metal oxide materials that exhibit charge and/or spin ordering. For example, perovskite ferrites [39] and nickelates [40–42] are known to exhibit static breathing distortions linked to charge ordering phenomena, and it was recently reported that nickelate superlattices exhibit differing charge- or spin-ordered states for different superlattice periodicities [42]. For these reasons, it would be interesting to explore the stabilization of such ordered states via thickness control in other transition metal oxide materials.

We thank H. D. Kim, S. W. Kim, S. Y. Kim, Y. Kim, T. Y. Koo, and C. H. Sohn for their assistance in the experiments, as well as J. S. Chung, I. Fisher, H. Y. Hwang, H. Jin, B. Keimer, D. Sando, M. Souliou, M. Le Tacon, and S. Uchida for helpful discussions. The crystal structure images were generated using the 3D visualization software package VESTA [43]. This work was supported by IBS-R009-D1. Synchrotron XRD measurements were performed at the Pohang Light Source 3A beamline.

G. K., M. N., and M. K. contributed equally to this work.

*minukim@snu.ac.kr
†twnoh@snu.ac.kr

[1] A. W. Sleight, J. L. Gillson, and P. E. Bierstedt, Solid State Commun. **17**, 27 (1975).
[2] R. J. Cava, B. Batlogg, J. J. Krajewski, R. Farrow, L. W. Rupp, Jr, A. E. White, K. Short, W. F. Peck, and T. Kometani, Nature (London) **332**, 814 (1988).
[3] D. G. Hinks, B. Daborowski, J. D. Jorgensen, A. W. Mitchell, D. R. Richards, S. Pei, and D. Shi, Nature (London) **333**, 836 (1988).
[4] S. Uchida, K. Kitazawa, and S. Tanaka, Phase Transit. **8**, 95 (1987).
[5] B. A. Baumert, J. Supercond. **8**, 175 (1995).
[6] A. W. Sleight, Physica C (Amsterdam) **514**, 152 (2015).
[7] D. E. Cox and A. W. Sleight, Solid State Commun. **19**, 969 (1976).
[8] T. M. Rice and L. Sneddon, Phys. Rev. Lett. **47**, 689 (1981).
[9] E. Jurczek and T. M. Rice, Europhys. Lett. **1**, 225 (1986).
[10] L. F. Mattheiss and D. R. Hamann, Phys. Rev. B **28**, 4227 (1983).
[11] L. F. Mattheiss and D. R. Hamann, Phys. Rev. Lett. **60**, 2681 (1988).
[12] T. Thonhauser and K. M. Rabe, Phys. Rev. B **73**, 212106 (2006).
[13] C. Franchini, G. Kresse, and R. Podloucky, Phys. Rev. Lett. **102**, 256402 (2009).
[14] C. Franchini, A. Sanna, M. Marsman, and G. Kresse, Phys. Rev. B **81**, 085213 (2010).
[15] D. Korotin, V. Kukolev, A. V. Kozhevnikov, D. Novoselov, and V. I. Anisimov, J. Phys. Condens. Matter **24**, 415603 (2012).
[16] Z. P. Yin, A. Kutepov, and G. Kotliar, Phys. Rev. X **3**, 021011 (2013).
[17] V. Vildosola, F. Güller, and A. M. Llois, Phys. Rev. Lett. **110**, 206805 (2013).
[18] T. Bazhirov, S. Coh, S. G. Louie, and M. L. Cohen, Phys. Rev. B **88**, 224509 (2013).
[19] P. V. Balachandran and J. M. Rondinelli, Phys. Rev. B **88**, 054101 (2013).
[20] K. Foyevtsova, A. Khazraie, I. Elfimov, and G. A. Sawatzky, Phys. Rev. B **91**, 121114 (2015).
[21] S. Pei, J. D. Jorgensen, B. Dabrowski, D. G. Hinks, D. R. Richards, A. W. Mitchell, J. M. Newsam, S. K. Sinha, D. Vaknin, and A. J. Jacobson, Phys. Rev. B **41**, 4126 (1990).
[22] M. Braden, W. Reichardt, E. Elkaim, J. P. Lauriat, S. Shiryaev, and S. N. Barilo, Phys. Rev. B **62**, 6708 (2000).
[23] See Supplemental Material at http://link.aps.org/supplemental/10.1103/PhysRevLett.115.226402 for details on sample growth and characterization, and additional Raman spectroscopic measurements. This material includes Refs. [24] and [25].
[24] D. Necas and P. Klapetek, Central Eur. J. Phys. **10**, 181 (2012).
[25] D. T. Marx, P. G. Radaelli, J. D. Jorgensen, R. L. Hitterman, D. G. Hinks, S. Pei, and B. Dabrowski, Phys. Rev. B **46**, 1144 (1992).
[26] E. S. Hellman, E. H. Hartford, and T. T. M. Palstra, Physica C (Amsterdam) **162–164**, 633 (1989).
[27] H. Yamamoto, K. Aoki, A. Tsukada, and M. Naito, Physica C (Amsterdam) **412–414**, 192 (2004).
[28] K. Inumaru, H. Miyata, and S. Yamanaka, Phys. Rev. B **78**, 132507 (2008).
[29] S. Tajima, M. Yoshida, N. Koshizuka, H. Sato, and S. Uchida, Phys. Rev. B **46**, 1232 (1992).
[30] H. Sato, S. Tajima, H. Takagi, and S. Uchida, Nature (London) **338**, 241 (1989).
[31] R. P. S. M. Lobo and F. Gervais, Phys. Rev. B **52**, 13294 (1995).
[32] T. Nishio, J. Ahmad, and H. Uwe, Phys. Rev. Lett. **95**, 176403 (2005).
[33] P. Giraldo-Gallo, Y. Zhang, C. Parra, H. C. Manoharan, M. R. Beasley, T. H. Geballe, M. J. Kramer, and I. R. Fisher, Nat. Commun. **6**, 8231 (2015).
[34] T. Ando, A. B. Fowler, and F. Stern, Rev. Mod. Phys. **54**, 437 (1982).
[35] K. Yoshimatsu, K. Horiba, H. Kumigashira, T. Yoshida, A. Fujimori, and M. Oshima, Science **333**, 319 (2011).
[36] M. Kim, C. Bell, Y. Kozuka, M. Kurita, Y. Hikita, and H. Y. Hwang, Phys. Rev. Lett. **107**, 106801 (2011).
[37] J. J. Lee, F. T. Schmitt, R. G. Moore, S. Johnston, Y.-T. Cui, W. Li, M. Yi, Z. K. Liu, M. Hashimoto, Y. Zhang, D. H. Lu, T. P. Devereaux, D.-H. Lee, and Z.-X. Shen, Nature (London) **515**, 245 (2014).
[38] J.-F. Ge, Z.-L. Liu, C. Liu, C.-L. Gao, D. Qian, Q.-K. Xue, Y. Liu, and J.-F. Jia, Nat. Mater. **14**, 285 (2015).
[39] P. M. Woodward, D. E. Cox, E. Moshopoulou, A. W. Sleight, and S. Morimoto, Phys. Rev. B **62**, 844 (2000).
[40] J. A. Alonso, J. L. García-Muñoz, M. T. Fernández-Díaz, M. A. G. Aranda, M. J. Martínez-Lope, and M. T. Casais, Phys. Rev. Lett. **82**, 3871 (1999).
[41] H. K. Yoo, S. I. Hyun, L. Moreschini, Y. J. Chang, D. W. Jeong, C. H. Sohn, Y. S. Kim, H.-D. Kim, A. Bostwick, E. Rotenberg, J. H. Shim, and T. W. Noh, arXiv:1309.0710v2.
[42] M. Hepting, M. Minola, A. Frano, G. Cristiani, G. Logvenov, E. Schierle, M. Wu, M. Bluschke, E. Weschke, H.-U. Habermeier, E. Benckiser, M. Le Tacon, and B. Keimer, Phys. Rev. Lett. **113**, 227206 (2014).
[43] K. Momma and F. Izumi, J. Appl. Crystallogr. **44**, 1272 (2011).